ELSEVIER

21 November 1994

PHYSICS LETTERS A

Physics Letters A 195 (1994) 31–37

Precision of quantum tomographic detection of radiation

G.M. d'Ariano [a,b], Chiara Macchiavello [a,1], Matteo G.A. Paris [a,2]

[a] *Dipartimento di Fisica "Alessandro Volta", Via A. Bassi 6, I-27100 Pavia, Italy*

[b] *Istituto Nazionale di Fisica Nucleare, Sezione di Pavia, Via A. Bassi 6, I-27100 Pavia, Italy*

Received 25 May 1994; revised manuscript received 5 October 1994; accepted for publication 10 October 1994
Communicated by P.R. Holland

Abstract

Homodyne tomography provides an experimental technique for reconstructing the density matrix of the radiation field. Here we analyze the tomographic precision in recovering observables like the photon number, the quadrature, and the phase. We show that tomographic reconstruction, despite providing a complete characterization of the state of the field, is generally much less efficient than conventional detection techniques.

1. Introduction

Quantum tomography provides the maximum achievable information on a given quantum radiation state, as, in principle, the knowledge of the density matrix allows one to calculate all expectation values for any desired observable. This means that quantum tomography is at the same time a phase detection, a quadrature detection, a photon number detection, and so on. The possibility of experimentally reconstructing the density matrix of a single mode of the radiation field has been firstly demonstrated by Raymer et al. in Ref. [1]. Very recently we have obtained a greatly improved reconstruction algorithm, which also provides the experimental error bars for all detected matrix elements [2]. Hence, it is now possible to evaluate the precision of this novel kind of detection, and to compare it with those of conventional single-observable schemes: this problem will be addressed in the present paper for a single mode of the radiation field.

The principle of quantum tomography relies on the possibility of obtaining the s-ordering Wigner function $W_s(\alpha,\bar{\alpha})$ from an ensemble of repeated measurements of the quadrature $\hat{a}_\phi = \frac{1}{2}(a\,\mathrm{e}^{-\mathrm{i}\phi} + a^\dagger\,\mathrm{e}^{\mathrm{i}\phi})$ at various phases ϕ relative to the local oscillator. From the probability distributions $p(x,\phi)$ of the outcomes x of $\hat{a}_\phi$ the Wigner function $W_s(\alpha,\bar{\alpha})$ is recovered through the formula [3]

$$W_s(\alpha,\bar{\alpha}) = \frac{1}{4}\int_{-\infty}^{\infty} \mathrm{d}\eta\,|\eta| \int_{-\infty}^{\infty} \mathrm{d}x \int_0^{\pi} \frac{\mathrm{d}\phi}{\pi}\, p(x,\phi)\exp\{\tfrac{1}{8}s\eta^2 + \mathrm{i}\eta[x - \mathrm{Re}\,(\alpha\,\mathrm{e}^{\mathrm{i}\phi})]\}\,. \tag{1}$$

[1] E-mail: macchiavello@pv.infn.it.
[2] E-mail: paris@pv.infn.it.

SSDI 0375-9601(94)00809-4

In Eq. (1) the inner integrals over x and ϕ can be estimated as averages on a finite set of experimental data only for strictly negative s, due to divergence of the outer Fourier transform over η. For $s \geqslant 0$, the probability $p(x,\phi)$ must be provided in analytic form, thus requiring a smoothing procedure on experimental data. Such smoothing is the basis of the original reconstruction algorithm [1], where the symmetrical-ordering Wigner function $W_0(\alpha,\bar{\alpha})$ is evaluated from filtered back-projected data, whereas the density matrix itself is subsequently obtained through further integral transforms[3]. Besides requiring much numerical effort in performing smoothing and subsequent integration steps, this method needs a sort of *a priori* assumption on the detected state in order to tune the filtering parameter.

Contrarily to the case $s \geqslant 0$, for $s < 0$ it is possible to evaluate $W_s(\alpha,\bar{\alpha})$ in the form of simple averages on data, without any a priori assumption, and with the great advantage of obtaining reliable statistics for experimental error bars. This second option is that adopted in our method [2]: it will be briefly recalled in the next section.

2. Non-filtered reconstruction algorithm

For $s = -1$ the Wigner function coincides with the Husimi Q-function $Q(\alpha,\bar{\alpha})$ (the probability distribution for antinormally ordered operator products) which itself is the generating function of the density matrix elements $\rho_{n,m}$ in the number representation, namely

$$\rho_{n,m} = \frac{1}{\sqrt{n!m!}} \frac{\partial^n}{\partial \bar{\alpha}^n} \frac{\partial^m}{\partial \alpha^m} [Q(\alpha,\bar{\alpha}) \exp(|\alpha|^2)]|_{\alpha=\bar{\alpha}=0} . \tag{2}$$

After evaluating derivatives in Eq. (2) analytically, Eqs. (1) and (2) directly connect the matrix elements $\rho_{n,m}$ to simple averages on homodyne data. Let us denote by $\bar{\rho}_{n,m}$ the experimental mean value of $\rho_{n,m}$ obtained from Eqs. (1) and (2) when the integrals over x and ϕ are replaced with the corresponding experimental averages. Typically the average on the phase ϕ is evaluated by summing over F equally spaced values $\phi_f = f\pi/F$ ($f = 0,\ldots,F-1$). A lengthy but straightforward derivation leads to the following reconstruction formula,

$$\bar{\rho}_{n,n+d} = \sum_{m=0}^{[n+d/2]} \frac{1}{F} \sum_{f=0}^{F-1} \mathbf{R}^{(d)}_{nm}(\phi_f) \left\langle \mathbf{H}^{(d)}_{nm}(x) \right\rangle_{\phi_f} , \tag{3}$$

where $d \geqslant 0$, the brackets $\langle\ \rangle_{\phi_f}$ denote averaging over the subensemble of data for fixed phase $\phi = \phi_f$ (with experimental outcome x), $[z]$ is the integer part of z, and the averaged function $\mathbf{H}^{(d)}_{nm}(x)$ is given by

$$\mathbf{H}^{(d)}_{nm}(x) = \exp(-2x^2) x^{\langle d \rangle_2} \Phi\left(m - n - \tfrac{1}{2}d - \tfrac{1}{2}\langle d+1\rangle_2, \tfrac{1}{2} + \langle d\rangle_2; 2x^2\right) . \tag{4}$$

---

[3] The density matrix in the quadrature representation is obtained from $W_0(\alpha,\bar{\alpha})$ using the Fourier transform

$$\langle x + x'|\hat{\rho}|x - x'\rangle = \int_{-\infty}^{\infty} \mathrm{d}y\ \mathrm{e}^{2\mathrm{i}x'y} W_0(x + \mathrm{i}y, x - \mathrm{i}y) .$$

Then the change to the number representation requires the following two additional integrals,

$$\langle n|\hat{\rho}|m\rangle = \frac{1}{\sqrt{\pi \times 2^n \times 2^m n!m!}} \int_{-\infty}^{\infty} \mathrm{d}x \int_{-\infty}^{\infty} \mathrm{d}x' \exp[-\tfrac{1}{2}(x^2 + x'^2)] H_n(x) H_m(x') \langle x|\hat{\rho}|x'\rangle ,$$

where $H_n(x)$ is the Hermite polynomial of degree n.

In Eq. (4) the notation $\langle z\rangle_2$ denotes the rest of the division $z/2$, whereas $\Phi(\alpha,\beta;z)$ is the confluent hypergeometric function of z with parameters α, β [4]. The fixed matrix $\mathbf{R}^{(d)}_{nm}(\phi)$ in Eq. (3) is given by

$$\mathbf{R}^{(d)}_{nm}(\phi) = \left(2^{3/2}\mathrm{i}\right)^{\langle d\rangle_2} \frac{2^{n+d/2+1}}{\sqrt{n!(n+d)!}} (-\mathrm{i})^{2n+d} \sum_{j_1=0}^{n}\sum_{j_2=0}^{d} (-1)^{j_2} \binom{n}{j_1}\binom{d}{j_2} (2n+d-2j_1-j_2)!(2j_1+j_2)!$$
$$\times \sum_{l_1=0}^{n-j_1+\lfloor (d-j_2)/2\rfloor} \sum_{l_2=0}^{j_1+\lfloor j_2/2\rfloor} \frac{(-8)^{-l_1-l_2}(\cos\phi)^{2n+d-2j_1-j_2-2l_1}(\sin\phi)^{2j_1+j_2-2l_2}}{l_1!l_2!(2j_1+j_2-2l_2)!(2n+d-2j_1-j_2-2l_1)!}$$
$$\times \Gamma\left(n+\tfrac{1}{2}d-l_1-l_2+\tfrac{1}{2}\langle d\rangle_2+1\right)\delta_{m,l_1+l_2}\,. \qquad (5)$$

Despite the apparent complexity of Eqs. (3)–(5) the average in Eq. (3) is particularly suited to on-line data analysis: in fact, apart from the sum over data, the procedure requires just a single sum over m, whereas hypergeometric functions $\Phi(\alpha,\beta;z)$ are connected to each other iteratively, and the matrix $\mathbf{R}^{(d)}_{nm}(\phi_{\mathrm{f}})$ is stored in the machine before beginning experiments[4]. In Ref. [2] the method has been tested on a set of Monte Carlo simulated experiments: the resulting averages $\bar{\rho}_{n,m}$ are in excellent agreement with theoretical values, with deviations $\delta\rho_{n,m}$ Gaussian distributed around the averages. In Fig. 1 a sample histogram of the normalized deviations from theoretical values for the first 30^2 matrix elements is reported for a coherent state with $\langle n\rangle = 4$: the comparison with the standard Gaussian is striking, and shows that about 68% of deviations lie within one standard deviation, corresponding to an optimal χ^2 ($\chi^2 = (1/N^2)\sum_{n=0}^{N-1}\sum_{m=0}^{N-1}\delta\rho_{n,m}/\varepsilon_{n,m}$, where $\varepsilon_{n,m}$ is the error bar on $\rho_{n,m}$) slightly greater than one.

3. Comparison with conventional detection

Quantities as phase, field quadrature and photon number could be measured by detecting the density matrix, but also in a direct way by double homodyne[5], single homodyne, and direct photodetection respectively. Direct measurements, however, give only partial information about the quantum state of the field: one thus expects that quantum tomography, providing the maximum available information, should require much more measurements in order to achieve the same precision as single-observable detection.

In this section we compare the precision of quantum tomography with those of common detection methods. In making such a comparison we have to keep in mind that tomography always needs a set of many repeated measurements on the same field: hence, when comparing tomography with single-observable schemes, the same number of repeated measurements must be considered. In a scheme of N repeated measurements of the quantity x, accuracy δx rescales as $\delta x \propto N^{-1/2}$. The proportionality constant generally depends on the kind of detection[6], and for experimental Gaussian distributions around the average one has that $\delta x = \sqrt{\langle\Delta x^2\rangle/N}$, $\langle\Delta x^2\rangle$ being the variance of x. In practice, in order to evaluate δx one can take advantage of the central limit theorem, which assures that the partial average over a block of N_{b} data is always Gaussian distributed around the global average over many blocks (for large N_{b}). Thus, as usual, one evaluates precision by dividing the ensembles of data into subensembles (the "experiments"), and then calculates the r.m.s. deviation of the subensemble averages with respect to the global one.

---

[4] As an example, for a 32^2 truncated density matrix, and for $F = 27$ and 10^4 data for each phase, the CPU time for a single matrix element is 0.045 s in average, with our algorithm running on an AlphaVax machine.

[5] Double homodyne detection [5] is actually a density operator detection in the Husimi Q-function representation, however it does not trivially provide all information on the field, because the antinormal form of generic functions of the field operators does not always exist.

[6] If the outcomes $\bar{x}$ are distributed around the true value x according to the probability $p(\bar{x}|x)$, the error for N repeated measurements is always bounded by the Cramer–Rao relation $\delta x \geqslant (FN)^{-1/2}$, with F the Fisher information $F = \int \mathrm{d}\bar{x}\,[\partial_x p(\bar{x}|x)]^2/p(\bar{x}|x)$. For Gaussian distributed data one has $F = 1/\sigma^2$, with σ^2 being the variance of distribution, and the lower bound of precision is achieved. (See Ref. [6].)

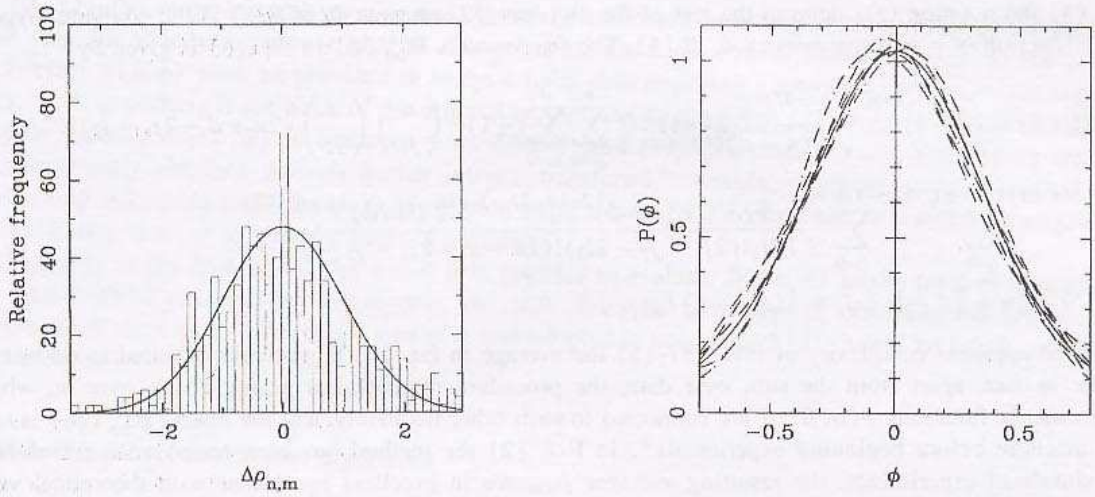

Fig. 1. Distribution of the normalized deviations from theoretical values ($\Delta\rho_{n,m} \equiv (\tilde{\rho}_{n,m} - \rho_{n,m})/\varepsilon_{n,m}$, $\varepsilon_{n,m}$ error bars on $\rho_{n,m}$) for the first 30^2 matrix elements of the density matrix. The quantum state is a coherent one with $\langle n\rangle = 4$. The histogram contains 1000 experiments (subensembles of data), each performed with $F = 27$ scanning phases and 200 measurements for each phase. The standardized Gaussian is superimposed.

Fig. 2. Reconstruction of the ideal phase probability distribution of a coherent state with $\langle n\rangle = 2$ mean photon number. Each curve corresponds to an experiment with $F = 27$ scanning phases and 100 measurements each. The solid line is the theoretical ideal distribution.

In the following we present results for different states of the radiation from simple Monte Carlo simulations of homodyne data. We compare quantum tomography with double homodyne phase detection, single homodyne quadrature detection, and photon number detection. In consideration that for customary shot noise one has the precision rescaling $\delta x \propto 1/\sqrt{\langle n\rangle}$ versus the average number of photons $\langle n\rangle$ (the same power law as versus the number of experiments N), all sensitivities will be given as a function of the total number of photons $N_T = N\langle n\rangle$ impinged in the apparatus.

3.1. Detection of the phase of the field

The probability distribution of an ideal phase detection is given by [7]

$$P(\varphi) = \frac{1}{2\pi}\sum_{n,m=0}^{\infty} e^{i(m-n)\varphi}\,\rho_{n,m}\,. \tag{6}$$

From the knowledge of the density matrix from tomographic detection one could evaluate the ideal phase probability (6), that otherwise cannot be directly measured in any known feasible experiment. Ideal phase probabilities have been reconstructed from tomographic data in Ref. [8], but the corresponding precision has not been analysed. In a tomographic experiment the reconstructed density matrix leads to an ideal phase distribution which, however, is still sensitive to errors on matrix elements, and thus is affected by fluctuations on the mean value. In Fig. 2 a sample of the ideal phase distributions resulting from five different tomographic simulated experiments is given for an input coherent state: it is evident that each experiment leads to a differently shifted distribution. The overall r.m.s. error for all experiments is $\delta\phi = 1.09 \times 10^{-2}$, which is much larger than $\sqrt{\langle\Delta\phi^2\rangle/5FN_b} = 4.23 \times 10^{-3}$ with $\langle\Delta\phi^2\rangle = 0.49$ the r.m.s. variance of each ideal phase distribution evaluated in the $[-\pi, +\pi]$ window (here each tomographic experiment has $F = 27$ phases, with $N_b = 100$ data each). In other words, even though the ideal phase distribution can be reconstructed from tomographic data, the variance

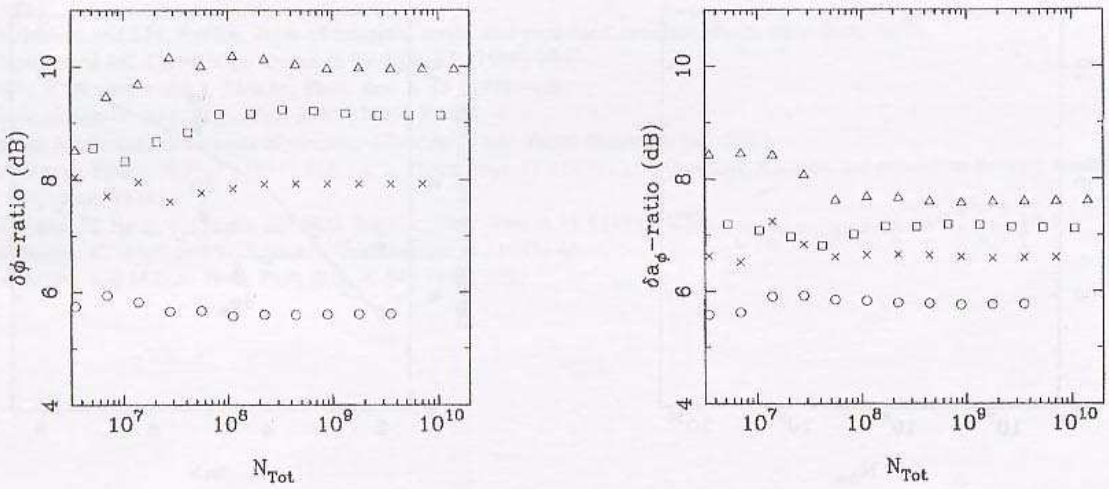

Fig. 3. Ratio (in dB) between phase precision from tomographic reconstruction and from a double homodyne detection as a function of the total mean number of photons impinged into the apparatus $N_T = N\langle n\rangle$, with N the total number of experiments. (For tomography N equals the number of phases F times the number data for each phase. Data are grouped into subensembles of 1000 elements each. In all this paper $F = 27$ is used.) Results for different coherent states are reported (circle: $\langle n\rangle = 2$, cross: $\langle n\rangle = 4$, square: $\langle n\rangle = 6$, triangle: $\langle n\rangle = 8$).

Fig. 4. Ratio between quadrature precision from tomographic reconstruction and from a homodyne detection as a function of the total mean number of photons impinged into the apparatus. Results for different coherent states are reported as in Fig. 3.

$\langle\Delta\phi^2\rangle$ of the distribution does not correspond to the actual precision of the method, and the resulting error $\delta\phi$ on the average phase is much larger than $\sqrt{\langle\Delta\phi^2\rangle/N}$.

As there is no feasible scheme for ideal phase detection (6), we compare tomographic results with those from a double homodyne phase detection [9] We find that five double homodyne experiments, with the same total impinged energy each, lead to an overall r.m.s. error $\delta\phi = 5.22 \times 10^{-3}$, which is much lower than the tomographic result, despite double homodyne being nonideal, and thus corresponds to a larger variance $\langle\Delta\phi^2\rangle = 0.61$. Hence the precision of double homodyne detection is better than the actual phase precision resulting from tomographic reconstruction, even though double homodyne is itself nonideal.

In Fig. 3 the ratio between tomographic and double homodyne phase sensitivities is plotted for various coherent states as a function of the total mean energy impinged into the apparatus. The noise added by tomography is apparent: the ratio between sensitivities is of several decibels. This ratio is almost independent of the total energy impinged in the apparatus, but depends on the mean photon number of the state. (Only slight differences between coherent and squeezed states have been found for the same mean photon numbers.)

3.2. *Field quadrature and photon number detection*

The same analysis previously performed for the phase is now considered as regards the field quadrature $\hat{a}_0 = \frac{1}{2}(a + a^\dagger)$ and the photon number. For the quadrature added noise is easily expected. In fact a single homodyne detection is already the direct field quadrature measurement and there is no need to detect also field quadratures at different phases to reconstruct its probability distribution. Quantum tomography adds noise also in the case of photon number detection. For the quadrature the ratio of sensitivities depends on the mean photon number of the input state (see Fig. 4), whereas for number detection such a dependence becomes very weak (see Fig. 5).

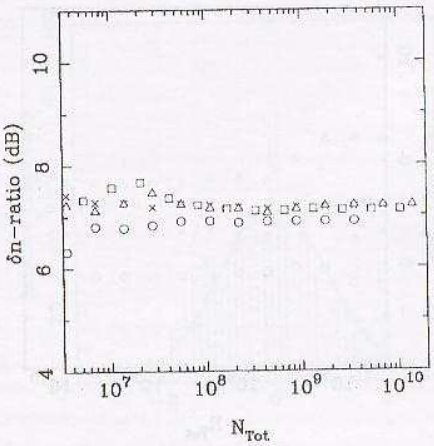

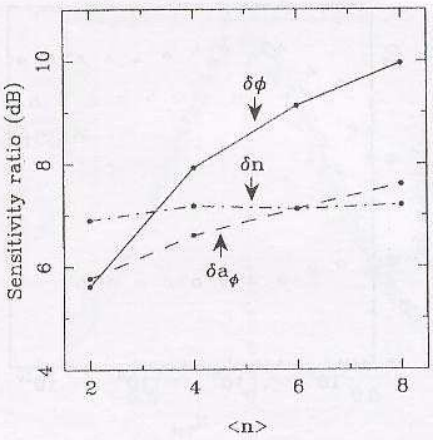

Fig. 5. Ratio between photon number precision from tomographic reconstruction and from a direct detection as a function of the total mean number of photons impinged into the apparatus. Results for different coherent coherent states are reported as in Fig. 3.

Fig. 6. Ratio between tomographic and single-observable detection sensitivities for all cases considered in Figs. 3–5, here as a function of the mean photon number of the input coherent states and for a very large number of measurements N (here $N_{tot} = \langle n \rangle \times 65536 \times 1000 \times 27$).

3.3. Asymptotic sensitivities for large number of experiments N

The ratio between tomographic and direct single-observable sensitivities is plotted in Fig. 6 for a very large number of repeated experiments $N = 65536 \times 1000 \times 27$ versus the number of photons of the input coherent state. In summary, we estimate that for large numbers of photons and input coherent states tomography adds more than 10 dB of noise in phase detection (with respect to double homodyne), 7 dB in photon number detection, and more than 8 dB in quadrature detection.

4. Conclusions

Tomographic reconstruction provides a complete characterization of the state of the field, however it requires a great number of repeated measures on the input state. By means of our reconstruction formula it is possible to estimate the experimental error bars for all density matrix elements, and hence the precision of tomography for all observables. We find that quantum tomography adds several dB of noise with respect to single-observable measurements, and becomes particularly noisy when phase is detected. Single-observable detection provides only partial information about the quantum state of the field, whereas quantum tomography gives the maximum knowable information: for this reason quantum tomography requires much more measures in order to achieve the same precision of direct methods. It is then a matter of convenience to choose between tomographic and single-observable techniques, also considering that tomography is not an efficient scheme when only one observable is of interest.

References

[1] D.T. Smithey, M. Beck, M.G. Raymer and A. Faridani, Phys. Rev. Lett. 70 (1993) 1244.
[2] G.M. d'Ariano, C. Macchiavello and M.G.A. Paris, Phys. Rev. A, in press.
[3] K. Vogel and H. Risken, Phys. Rev. A 40 (1989) 2847.

[4] I.S. Gradshteyn and I.M. Ryzhik, Table of integrals, series, and products (Academic Press, New York, 1980).
[5] N.G. Walker and J.E. Carrol, Opt. Quantum Electron. 18 (1986) 355;
J.W. Noh, A. Fougeres and L. Mandel, Phys. Rev. A 45 (1992) 424;
U. Leonhardt and H. Paul, Phys. Rev. A 47 (1993) R2460.
[6] H. Cramér, Mathematical methods of statistics (Princeton Univ. Press, Princeton, NJ, 1946).
[7] C.W. Helstrom, Found. Phys. 4 (1974) 453; Int. J. Theor. Phys. 11 (1974) 357; Quantum detection and estimation theory (Academic Press, New York, 1976).
[8] D.T. Smithey, M. Beck, J. Cooper and M.G. Raymer, Phys. Rev. A 48 (1993) 3159.
[9] M. Freyberger, K. Vogel and W. Schleich, Quantum Opt. 5 (1993) 65;
G.M. d'Ariano and M.G.A. Paris, Phys. Rev. A 49 (1994) 3022.